Journal of Materials Chemistry

Cite this: *J. Mater. Chem.*, 2011, **21**, 144

www.rsc.org/materials

PAPER

Improved visible light photocatalytic activity of titania doped with tin and nitrogen

Enjun Wang,[a] Tao He,*[b] Lusong Zhao,[a] Yongmei Chen[c] and Yaan Cao*[a]

Received 4th August 2010, Accepted 14th September 2010
DOI: 10.1039/c0jm02539a

Tin and nitrogen co-doped titania has been prepared by a hydrolysis precipitation method and studied by X-ray diffraction, X-ray photoelectron spectroscopy, diffuse reflectance UV-vis absorption spectra, and photoluminescence. The surface area has been determined by using the BET method. Tin is incorporated into the TiO_2 crystal lattice in substitutional mode, while nitrogen is present as surface species. The resultant energy levels of tin doping and nitrogen surface states are located inside the bandgap, which are close to the conduction and valence bands, respectively. Hence, co-doping of tin and nitrogen can greatly enhance the absorption in the visible light region and inhibit the recombination of photogenerated charge carriers, leading to a higher photocatalytic activity for the co-doped catalyst than pure TiO_2 and solely doped TiO_2 with nitrogen or tin for degradation of 4-chlorophenol under both visible and UV-light irradiation. This indicates that co-doping simultaneously with two foreign elements is a feasible way to improve the photocatalytic activity of TiO_2.

Introduction

Photocatalysis using titania (TiO_2) offers a viable approach for degradation of organic and inorganic pollutants in air and water due to its high oxidizing capacity, photostability, and non-toxicity.[1–4] However, TiO_2 exhibits photoresponse only to UV light because it is a wide-gap semiconductor (3.2 eV), which impedes the effective usage of solar illumination in practical applications. To efficiently use solar energy, recent research interest has been mainly focused on extending its response to visible light.[5–18] So far many efforts have been made in this field, such as surface modification,[5,6] doping TiO_2 with foreign ions,[7–12] combining TiO_2 with other semiconductors.[13–15] A breakthrough was made in 2001 with a visible-light photocatalyst *via* doping TiO_2 with nitrogen.[7] From then on, many experiments and theoretical work have been done on nitrogen-doped TiO_2,[16–27] indicating that this new catalyst exhibits a relatively high visible-light photocatalytic activity due to the creation of energy levels of doping and/or surface states above the valence band,[18–20] and/or bandgap narrowing.[7,21]

In addition, pristine TiO_2 exhibits a low quantum yield due to its relatively high recombination rate of photogenerated electron–hole pairs.[28,29] In an aqueous suspension system, only a few electrons in the conduction band have high enough energy that can overcome the potential barrier to reach the surface and be captured by the surface adsorbed O_2 since the energy bands of TiO_2 bend upward at the solid–liquid interface.[30] The majority of electrons will migrate to an opposite direction, the bulk of TiO_2, leading to an increase in the recombination probability of electron–hole pairs during the photocatalytic reaction. If a doping energy level can be introduced below the conduction band of TiO_2, therefore, the photogenerated electrons in the conduction band can transfer to the surface *via* this doping energy level, without crossing over the potential barrier, and take part in the photocatalytic process. This will facilitate the separation of photogenerated electron–hole pairs. Thus more photogenerated electrons and holes can contribute to the photocatalytic reaction, resulting in an enhancement of photocatalytic activity of the catalyst. This is confirmed by our previous work, in which Sn^{4+} ions were incorporated into the TiO_2 lattice in substitutional mode.[31,32] The doping energy level of Sn^{4+} ions is located at 0.4 eV below the conduction band of TiO_2, which allows an efficient transfer of photogenerated electrons to the surface and suppresses the recombination of photogenerated charge carriers. Furthermore, Sn^{4+} doping can also improve the photocatalytic performance of TiO_2 under visible light irradiation since it can lead to the visible-light response.[31,33]

Furthermore, the visible-light response and photocatalytic activity can be further improved for a photocatalyst with multi-dopants since the contribution can come from all the dopants. This has been demonstrated in several systems, such as (B,Ni),[14] (N,Fe),[25] (N,W),[27] (N,B),[34] (N,F)[35,36] and (C,F,N).[37] In this work, we present that a photocatalyst co-doped with nitrogen and tin can be prepared *via* a simple sol–gel method. Tin is incorporated into the TiO_2 crystal lattice in

[a]*Teda Applied Physics School, Institute of Physics, Nankai University, Tianjin, 300071, China. E-mail: caoyaan@yahoo.com; Fax: +86-22-66229310; Tel: +86-22-66229598*
[b]*National Center for Nanoscience and Technology, Beijing, 100190, China. E-mail: het@nanoctr.cn*
[c]*School of Science, Beijing University of Chemical Technology, Beijing, 100029, China*

substitutional mode, while nitrogen exists as surface species. Moreover, as expected, it exhibits a higher visible and UV-light photocatalytic activity than pure TiO_2, tin-doped TiO_2, and nitrogen-doped TiO_2. The mechanism is also discussed in this contribution.

Experimental

Catalyst preparation

All chemicals were of analytical grade. Milli-Q water (> 18.2 MΩ cm) was used for all experiments. Co-doped photocatalysts were prepared by using the following protocol. First, deionized water (1 mL) was mixed with anhydrous ethanol (40 mL) at room temperature, followed by the dropwise addition of tetrabutyltitanate ($Ti(OC_4H_9)_4$, 12 mL) to the solution under vigorous stirring. Concentrated hydrochloric acid (12 M) was used to adjust the pH to 0.5. Then 0.2 mL $SnCl_4$, 1 mL water, and 3 mL ammonia were added in sequence under stirring. A white precipitate formed immediately upon addition of ammonia. After aging at room temperature for 24 h, the resultant precipitate was dried at 100 °C, followed by annealing at 450 °C for 2.5 h. The obtained samples were denoted as N/Sn-TiO_2. Tin-doped TiO_2 (Sn-TiO_2), nitrogen-doped TiO_2 (N-TiO_2), and pure TiO_2 were prepared using the same procedure, but with the addition of the corresponding doping reagent.

Catalyst characterization

X-Ray diffraction (XRD) patterns were acquired on a Rigaku D/max 2500 X-ray diffraction spectrometer (Cu Kα, $\lambda = 1.54056$ Å) at a scan rate of 0.02° 2θ s^{-1}. The average crystal size was calculated using the Scherrer equation ($D = k\lambda/\beta\cos\theta$). After degassing at 180 °C, the BET surface area was determined *via* the measurement of nitrogen adsorption–desorption isotherms at 77 K (Micromeritics Automatic Surface Area Analyzer Gemini 2360, Shimadzu). X-Ray photoelectron spectroscopy (XPS) measurements were carried out with an ESCA Lab 220i-XL spectrometer by using an unmonochromated Al Kα X-ray source (1486.6 eV). All spectra were calibrated using the binding energy (BE) of the adventitious C1s peak at 284.6 eV. Diffuse reflectance UV-vis absorption spectra (UV-Vis DRS) were collected with a UV-vis spectrometer (U-4100, Hitachi). Photoluminescence (PL) spectra were acquired by using the 340 nm line of a nanosecond Nd:YAG laser (NL303G) as excitation source at room temperature.[38]

Photocatalytic reactivity test

Photocatalytic decomposition of 4-chlorophenol (4-CP) was used to evaluate the photocatalytic activity of the resultant catalyst, which was carried out using 10 mg of catalyst suspended in a 4-CP aqueous solution (40 mL, 5×10^{-5} mol L^{-1}) under visible and UV-light irradiation. A sunlamp (Philips HPA 400/30S, Belgium) was used directly for the UV-light photocatalytic reaction, while for visible-light photocatalysis a 400 nm cutoff filter was employed to remove the UV light. The reactor was perpendicular to the light beam and located 10 cm away from the light source. The 4-CP solution was continuously bubbled using O_2 gas at a flux of 5 mL min^{-1} under stirring at 25 ± 2 °C. The change in concentration of 4-CP was monitored by a UV-visible spectrometer (UV-1061PC, SHIMADZU) using 4-aminoantipyrine as the chromogenic reagent. The suspension was magnetically stirred in the dark for 30 min before photocatalytic reaction, which was long enough to reach the adsorption equilibrium of 4-CP. The control experiment was performed under identical conditions, but without a photocatalyst.

Results

XRD patterns

Fig. 1 shows the XRD patterns of TiO_2 (curve a), N-TiO_2 (curve b), Sn-TiO_2 (curve c), and N/Sn-TiO_2 (curve d) powders. It is found that the majority of the crystal phase is anatase for all of the samples.[27] The shape of the diffraction peaks of N-TiO_2 and N/Sn-TiO_2 is consistent with that of pure TiO_2. For Sn-TiO_2 sample (curve c), besides the anatase peaks, diffraction peaks at 26.6°, 33.9°, and 51.7° can also be observed, corresponding to the crystal planes of (110), (101), and (211) of SnO_2, respectively.[39] This indicates that a small amount of SnO_2 was formed in the Sn-TiO_2 sample during the doping process. However, the diffraction peaks of SnO_2 are not observed in the N/Sn-TiO_2 sample, suggesting that the addition of ammonia can inhibit the formation of SnO_2.

The inset in Fig. 1 is the enlarged XRD peaks of crystal plane (101) for all of the samples. Compared with the pure TiO_2, no shift of the peak position is observable for N-TiO_2 (curves b), while the peak of Sn-TiO_2 (curves c) shifts to lower diffraction angles ($\Delta \cong 0.08°$). It is noted that N/Sn-TiO_2 exhibits almost the same diffraction angle as that of Sn-TiO_2 (inset of Fig.1). The diffraction peaks of crystal planes (101), (200), and (105) in the

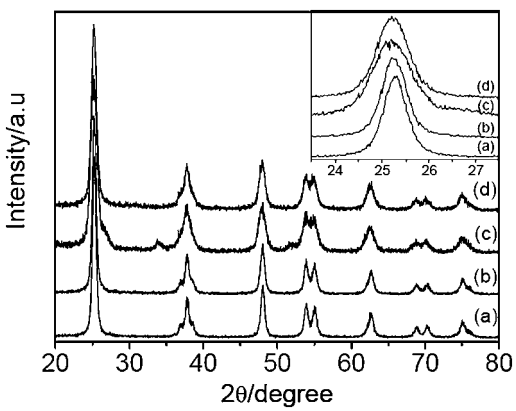

Fig. 1 XRD patterns of TiO_2 (a), N-TiO_2 (b), Sn-TiO_2 (c), and N/Sn-TiO_2 (d). Inset is the enlarged XRD peaks of crystal plane (101).

Table 1 Lattice parameter and crystal size of TiO_2, Sn-TiO_2, N-TiO_2, and N/Sn -TiO_2

Sample	$a = b$ (Å)	c (Å)	Cell volume (Å^3)	Crystal size (nm)	Specific surface area (m^2 g^{-1})
TiO_2	3.790	9.573	137.53	12.9	68.6
N-TiO_2	3.792	9.590	137.92	12.5	73.2
Sn-TiO_2	3.801	9.614	138.91	7.7	97.8
N/Sn-TiO_2	3.794	9.654	138.93	10.8	91.2

curves are used to determine the lattice parameter and crystal size of the samples, which are summarized in Table 1. It is found that the cell volume of N/Sn-TiO_2 and Sn-TiO_2 is much larger than that of pure TiO_2, while the cell volume of N-TiO_2 is almost the same as that of pure TiO_2. The detailed mechanism is discussed in the following sections.

The doping mode is primarily determined by two factors: electronegativity and ionic radius of the doping ions.[31] If the electronegativity and ionic radius of doping ions match those of the lattice ions in the oxide, the doping ions can substitute the lattice ions during the doping process.[31] Because the electronegativity and ionic radius of Sn^{4+} ions (1.8, 69 pm) are close to those of Ti^{4+} ions (1.5, 53 pm) in TiO_2,[31,40] it is feasible for Sn^{4+} ions to replace and occupy lattice Ti^{4+} ions. Since the ionic radius of Sn^{4+} ions is larger than that of lattice Ti^{4+} ions, the cell volume and lattice parameters of Sn-TiO_2 are larger than those of pure TiO_2. For the doping mode of nitrogen in N-TiO_2, since the ionic radius of the nitrogen ion (171 pm) is much larger than that of the oxygen ion (140 pm), a dramatic change in lattice parameter and cell volume would be expected if nitrogen were substituted into the lattice. However, an obvious increase in lattice parameter and cell volume is not observed after nitrogen doping according to XRD results. The doping of nitrogen into TiO_2 through the substitutional mode can thus be excluded. Hence, it is proposed here that nitrogen dopants exist as surface species. In the case of N/Sn-TiO_2, it seems the change in cell volume comes mainly from Sn dopants since the cell volume of N/Sn-TiO_2 is almost the same as that of Sn-TiO_2. Therefore, according to the results of XRD, it is reasonable to speculate that tin can incorporate into the TiO_2 matrix in substitutional mode and nitrogen exists as surface species, which is confirmed by XPS results shown below.

In addition, it is noted that the size of N-TiO_2 nanoparticles is similar to that of pure TiO_2 (Table 1), indicating that nitrogen doping has almost no influence on the grain growth of N-TiO_2. Tin doping can remarkably inhibit the grain growth of Sn-TiO_2 since the crystal size of Sn-TiO_2 is smaller than that of pure TiO_2. The specific surface area ranks in the order of TiO_2 < N-TiO_2 < N/Sn-TiO_2 < Sn-TiO_2 (Table 1), which agrees with the trend for the change in crystal size of the samples. The fact that Sn-TiO_2 exhibits a lower photocatalytic activity than N/Sn-TiO_2 and N-TiO_2 although it has the largest specific surface area indicates that here the doping of N and Sn, rather than the increase in surface area, plays a major role in the enhancement of photocatalytic activity.

XPS analysis

XPS measurements are used to investigate the chemical states of N and Sn in N-TiO_2, Sn-TiO_2, and N/Sn-TiO_2 samples. Fig. 2 shows the N1s peaks of N-TiO_2 and N/Sn-TiO_2, in which broad peaks centered at about 399.4 eV (N-TiO_2) and 400.4 eV (N/Sn-TiO_2) are observed. These two peaks are much higher than the typical binding energy (BE) of 396.9 eV in TiN,[41] indicating that the N atoms in N-TiO_2 and N/Sn-TiO_2 interact strongly with O atoms.[18] Therefore the BE of 399.4 and 400.4 eV here are attributed to the oxidized nitrogen similar to NO_x species, meaning that Ti–N–O linkage possibly formed on the surface of N-TiO_2 and N/Sn-TiO_2.[42–46] Furthermore, it is highly possible that some N–O species coordinate with tin to form the Sn–N–O linkage on the surface of N/Sn-TiO_2. For the latter case, the electron density of N atoms in Sn–N–O is lower than that in Ti–N–O since the electronegativity of Sn is larger than that of Ti,[31] which may explain why the BE of nitrogen surface species for N/Sn-TiO_2 (400.4 eV) is higher than that for N-TiO_2 (399.4 eV).

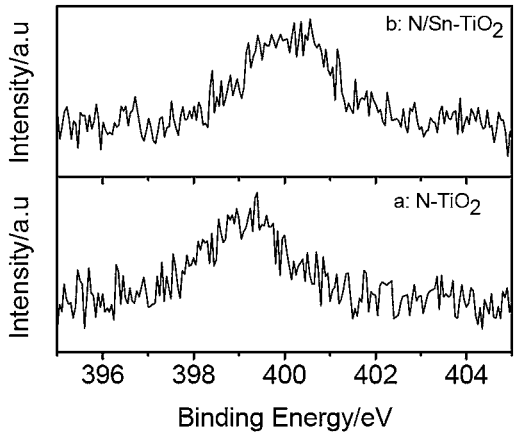

Fig. 2 N1s XPS spectra of N-TiO_2 (a) and N/Sn-TiO_2 (b).

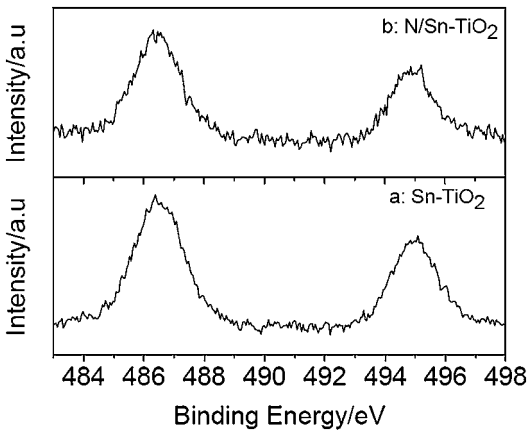

Fig. 3 Sn3d XPS spectra of Sn-TiO_2 (a) and N/Sn-TiO_2 (b).

Fig. 3 presents the Sn3d spectra of Sn-TiO_2 and N/Sn-TiO_2. The doublet peak around 486.4 eV and 494.9 eV is ascribed to $Sn3d_{5/2}$ and $Sn3d_{3/2}$, respectively, which arises from the doping Sn^{4+} ions that substitute lattice Ti in Sn-TiO_2 and N/Sn-TiO_2 samples because the $Sn3d_{5/2}$ peak falls between that for SnO_2 (486.7 eV) and metallic Sn (485.0 eV).[31,47] According to XPS and XRD results, therefore, nitrogen is present as surface species in N/Sn-TiO_2 and tin incorporates into TiO_2 lattice in substitutional mode. According to XPS spectra, moreover, the Ti : Sn and Ti : N ratio in N/Sn-TiO_2 sample is 1 : 0.034 and 1 : 0.059, respectively.

UV-Vis DRS

Fig. 4 gives UV-Vis DRS absorption spectra of TiO_2, N-TiO_2, Sn-TiO_2, and N/Sn-TiO_2 samples. Pure TiO_2 only exhibits a strong absorption in the UV region that is attributed to the band-to-band transition.[27] Compared with the pure TiO_2, N-TiO_2 presents a small hump at around 450 nm tailing the visible-light region, which is a typical absorption feature of

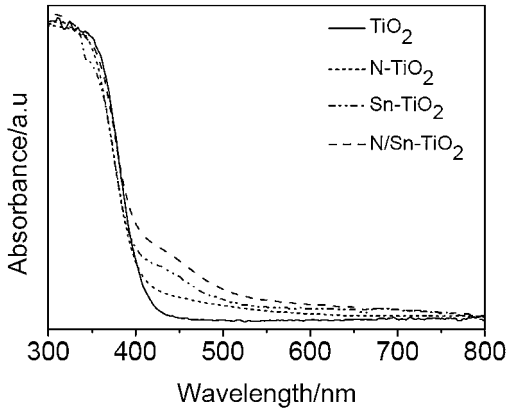

Fig. 4 UV-Vis DRS absorption spectra of TiO_2, N-TiO_2, Sn-TiO_2, and N/Sn-TiO_2.

nitrogen-doped TiO_2 and arises from the electron transition from surface state of NO_x species to the conduction band of TiO_2.[48,49]

As shown in Fig. 4, Sn-TiO_2 shows a distinct hump at 450 nm, which agrees with our previous work.[31] Since the doping energy level of Sn^{4+} ions is located at 0.4 eV below the conduction band, it is suggested that the visible-light absorption of Sn-TiO_2 arises from the electronic transition from valance band to this doping energy level.

The N/Sn-TiO_2 samples show a strong absorption in the visible range from 400 to 600 nm (Fig. 4), which is stronger than N-TiO_2 and Sn-TiO_2 because the contribution is from both the nitrogen surface species and substitutionally doped tin. This means that nitrogen and tin co-doped TiO_2 catalysts are more sensitive to the visible light than TiO_2, Sn-TiO_2, and N-TiO_2.

Photoluminescence spectra

Fig. 5 shows PL emission spectra of pure TiO_2, N-TiO_2, Sn-TiO_2, and N/Sn-TiO_2. Two peaks around 480 and 525 nm are observed

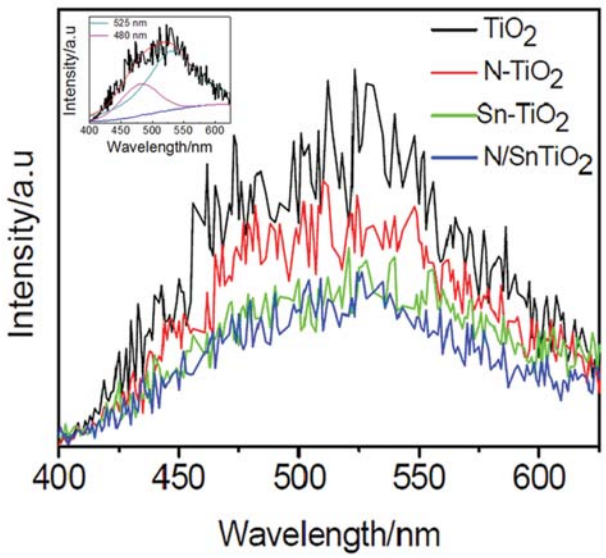

Fig. 5 Photoluminescence emission spectra of TiO_2 (black), N-TiO_2 (red), Sn-TiO_2 (green), and N/Sn-TiO_2 (blue). Inset shows the fitting results for the TiO_2 sample, from which two peaks can clearly be observed.

for TiO_2, which is attributed respectively to the transition from oxygen vacancies with two-trapped electrons and one-trapped electron to the valence band of TiO_2.[36,50–52] The energy levels relate to these two types of oxygen vacancies are located at 0.51 eV and 0.82 eV below the conduction band of TiO_2, respectively.[50,52] Thus, the origin of PL is explained as follows.

First, the photogenerated electrons in the conduction band can fall into the oxygen vacancies through a non-irradiative process, and then recombine with the photogenerated holes in the valence band, accompanied by the fluorescence emission. Compared with pure TiO_2, the emission intensity is weakened significantly for N-TiO_2 and Sn-TiO_2, while further weakened for N/Sn-TiO_2. This implies that the recombination of charge carriers is effectively suppressed upon doping of N and/or Sn.

A lower PL intensity of N-TiO_2 can be attributed to the capture of photogenerated holes by surface states (surface nitrogen species). The effective quenching of PL for Sn-TiO_2 is due to the formation of the doping energy level of Sn^{4+} ions, located at 0.4 eV below the conduction band in the Sn-TiO_2 sample. Since the doping energy level of Sn^{4+} ions is higher than those of oxygen vacancies (0.51 and 0.82 eV below the conduction band), the photogenerated electrons in the conduction band are inclined to move from the conduction band to the doping energy level of Sn^{4+} ions, rather than to the oxygen vacancies. As a result, the emission intensity originated from the transition from oxygen vacancies to the valence band decreases greatly after doping of Sn^{4+} ions. For N/Sn-TiO_2 samples, the separation of photogenerated holes and electrons is enhanced due to the contribution from both the nitrogen surface species and substitutionally doped tin, resulting in a much stronger suppressed recombination of photogenerated carriers and, thus, the lowest luminescence intensity for N/Sn-TiO_2 among all of the samples.

Photocatalytic activity

The photodegradation of 4-chlorophenol (4-CP) is used to evaluate the photocatalytic activity of TiO_2, N-TiO_2, Sn-TiO_2, and N/Sn-TiO_2. The adsorption curves in the dark indicate that the adsorption for all the samples can reach equilibrium after 30 min (Fig. 6c). The adsorption equilibrium amount for 10 mg of TiO_2, N-TiO_2 and Sn-TiO_2 samples is almost the same (4×10^{-8} mol) by coincidence, and it is 8×10^{-8} mol for 10 mg N/Sn-TiO_2. For all the samples, the $\ln(c_0/c)$ value of 4-CP shows a linear relationship *versus* irradiation time, suggesting that the photodegradation may be a pseudo-first-order reaction. The photocatalytic results under both visible and UV light are given in Fig. 6 and Tables 2 and 3. The 4-CP is hardly photo-degraded in the control experiment (photolysis of 4-chlorophenol), regardless of visible or UV-light irradiation. The pure TiO_2 photocatalyst shows a very low photocatalytic activity under visible-light irradiation ($\lambda > 400$ nm), while N-TiO_2 and Sn-TiO_2 exhibit a relatively high visible-light activity. N/Sn-TiO_2 has an even higher visible-light activity than N-TiO_2 and Sn-TiO_2, for which 49.1% of 4-CP can be degraded after 8 h of visible-light irradiation. The photodegradation rate and specific photocatalytic activity of N/Sn-TiO_2 are about four times those of pure TiO_2, and about two times those of N-TiO_2, indicating that co-doping TiO_2 with nitrogen and tin is an effective way for preparing TiO_2-based catalysts with a high visible-light photoactivity. The

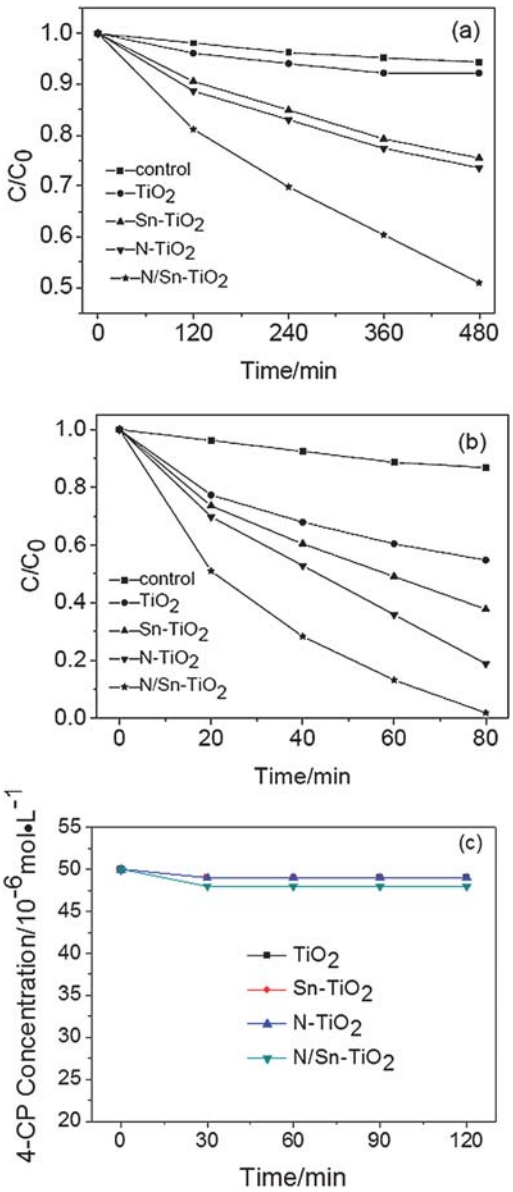

Fig. 6 Photodegradation of 4-CP under visible (a), UV-light irradiation (b), and adsorption curve under dark for 10 mg sample (c).

Table 2 Photodegradation of 4-CP under visible-light irradiation (λ > 400 nm)

Sample	4-CP Degraded [a] $(c_0 - c)/c_0$ (%)	k (min^{-1}) [b]	$t_{1/2}$ (min)	Specific photocatalytic activity (mol g^{-1} h^{-1})
Control[c]	5.7	1.14×10^{-4}	6063	—
TiO_2	15.1	3.44×10^{-4}	1987	5.45×10^{-6}
Sn-TiO_2	24.5	5.83×10^{-4}	1161	9.08×10^{-6}
N-TiO_2	26.4	6.28×10^{-4}	1066	1.09×10^{-5}
N/Sn-TiO_2	49.1	1.38×10^{-3}	487	1.82×10^{-5}

[a] After reaction for 8 h. [b] Apparent rate constant deduced from linear fitting of $\ln(c_0/c)$ *versus* reaction time. [c] The blank was the photolysis of 4-chlorophenol.

Table 3 Photodegradation of 4-CP under UV-light irradiation

Sample	4-CP degraded [a] $(c_0 - c)/c_0$ (%)	k (min^{-1})[b]	$t_{1/2}$ (min)	Specific photocatalytic activity (mol g^{-1} h^{-1})
Control	13.2	1.80×10^{-3}	377	—
TiO_2	45.3	7.30×10^{-3}	86	7.62×10^{-5}
Sn-TiO_2	62.2	1.18×10^{-2}	56	9.80×10^{-5}
N-TiO_2	81.0	2.02×10^{-2}	37	1.23×10^{-4}
N/SnTiO_2	98.1	4.86×10^{-2}	20	1.67×10^{-4}

[a] After reaction for 80 min. [b] Apparent rate constant deduced from linear fitting of $\ln(c_0/c)$ *versus* reaction time.

photocatalytic activity under UV-light irradiation exhibits the same order as that under visible-light irradiation, *i.e.*, N/Sn-TiO_2 > N-TiO_2 > Sn- TiO_2 > TiO_2 (Tables 2 and 3).

Discussion

Based on the aforementioned results, the reason that N/Sn-TiO_2 exhibits a high photodegradation capacity of 4-CP under both visible and UV light can be explained using the scheme shown in Fig. 7. Pure TiO_2 has a very low visible-light (λ > 400 nm) photodegradation capacity due to its large bandgap (3.2 eV, process A). After co-doping with tin and nitrogen, electrons can be excited simultaneously from valence band to Sn^{4+} doping energy level (process B), and from the surface states energy level (formed due to nitrogen surface species) to the conduction band (process C). Meanwhile, it is possible for photogenerated electrons at the conduction band to fall into the doping energy level of Sn^{4+}, located at 0.4 eV below the conduction band.[31] The photogenerated electrons can also transfer from the conduction band and Sn^{4+} doping energy level to the surface of nanoparticles.

Because the energy level of O_2/O_2^- is lower than that of the doping energy level of Sn^{4+} ions and the conduction band (Fig. 7), photogenerated electrons are directly captured by the adsorbed O_2 molecules on the surface of N/Sn-TiO_2 to form O_2^- active species during the photocatalytic process (eqn (1)).[2,31] The resultant O_2^- can react with the photogenerated electrons to form H_2O_2 (eqn (2)), which can further react with photogenerated electrons to produce OH^- and the hydroxyl free radical OH• (eqn (3)). The obtained OH^- can react with photogenerated holes to generate active species OH• (eqn (4)). Both O_2^- and OH• can oxidize 4-CP molecules absorbed on the catalyst surface.[1] In addition, photogenerated holes at both the valance band and surface states can directly oxidize 4-CP, or be trapped by surface hydroxyl to form active species OH•. Eventually, 4-CP molecules are photodegraded into CO_2 and H_2O. For solely doped TiO_2, however, only process B exists for Sn-TiO_2 under visible-light irradiation, and process C for N-TiO_2. Therefore, co-doping with nitrogen and tin can increase the quantity of photoinduced electrons and holes, compared with pure and solely doped TiO_2. As discussed above (Fig. 5), moreover, N/Sn-TiO_2 has the highest efficiency for the separation of photogenerated electrons and holes among all of the samples and, accordingly, the lowest recombination rate. As a result,

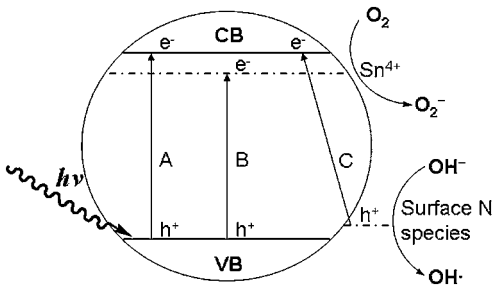

Fig. 7 Scheme of photocatalytic mechanism of nitrogen and tin co-doped TiO_2.

more photogenerated electrons and holes will contribute to the photocatalytic process, resulting in a higher photocatalytic activity than that of pure TiO_2, N-TiO_2, and Sn-TiO_2.

$$O_2 + e \rightarrow O_2^- \quad (1)$$

$$O_2 + 2H^+ + 2e \rightarrow H_2O_2 \quad (2)$$

$$H_2O_2 + e \rightarrow OH^- + HO\bullet \quad (3)$$

$$OH^- + h^+ \rightarrow HO\bullet \quad (4)$$

In the case of UV light, process A is allowed for all of the samples. For pure TiO_2, due to the existence of the potential barrier of TiO_2 surface at the liquid–solid interface, the photogenerated electrons at the conduction band would migrate to TiO_2 bulk along the band-bending direction rather than transfer to the TiO_2 surface over the potential barrier, which increases the probability of electron–hole recombination. Compared with pure TiO_2, N-TiO_2 and Sn-TiO_2, the photocatalytic activity of N/Sn-TiO_2 under UV-light irradiation is improved due to existence of the energy levels of both doping Sn^{+4} ions and surface state of NO_x species. Since the doping energy level of Sn^{+4} is located at 0.4 eV below the conduction band, the photogenerated electrons at the conduction band will directly transfer to the catalyst surface *via* this Sn^{+4} doping energy level, and then captured by the adsorbed O_2 molecules on the surface of N/Sn-TiO_2 to form O_2^- active species, which will further degrade 4-CP molecules adsorbed on the surface. Meanwhile, the photogenerated holes at the valence band can transfer to the surface state (surface NO_x species), and then oxidize 4-CP molecules adsorbed on the N/Sn-TiO_2 surface during the photocatalytic process. This effectively facilitates the separation of photogenerated electrons and holes and thereby inhibits their recombination, resulting in more electrons and holes that can contribute to the photocatalytic reaction. Compared with pure TiO_2, N-TiO_2, and Sn-TiO_2, as a result, the photocatalytic activity of N/Sn-TiO_2 is also improved under UV-light irradiation.

Conclusions

In summary, a new type of TiO_2-based photocatalyst (N/Sn-TiO_2) has been successfully prepared by co-doping TiO_2 with tin and nitrogen using a simple sol–gel technique, which exhibits a higher photocatalytic activity than pure TiO_2, nitrogen-doped TiO_2, and tin-doped TiO_2 under both visible and UV-light irradiation due to the contribution from both nitrogen surface species and substitutionally doped tin. This implies that co-doping with two foreign ions, metal and nonmetal, is a more efficient way to improve the photocatalytic activity of TiO_2 than doping with just one type of ion. It is expected that detailed studies on the co-doped TiO_2 catalyst in the ongoing research, especially more precise control over the alignment of energy levels, will afford a viable way to develop TiO_2-based visible-light photocatalysts suitable for practical applications, as well as leading to improved catalyst design.

Acknowledgements

This work was supported by National Natural Science Foundation of China (No. 50872056 and No. 51072082). T. H. thanks National Research Fund for Fundamental Key Projects No. 973 (2011CB933200) and the Hundred-Talent Program of Chinese Academy of Sciences.

Notes and references

1 A. L. Linsebigler, G. Lu and J. T. Yates Jr., *Chem. Rev.*, 1995, **95**, 735.
2 M. R. Hoffmann, S. T. Martin, W. Choi and D. W. Bahnemannt, *Chem. Rev.*, 1995, **95**, 69.
3 X. B. Chen and S. S. Mao, *Chem. Rev.*, 2007, **107**, 2891.
4 A. Fujishima, X. T. Zhang and D. A. Tryk, *Surf. Sci. Rep.*, 2008, **63**, 515.
5 M. Zhang, C. C. Chen, W. H. Ma and J. C. Zhao, *Angew. Chem., Int. Ed.*, 2008, **47**, 9730.
6 G. Granados-Oliveros, E. A. Páez-Mozo, F. M. Ortega, C. Ferronato and J. Chovelon, *Appl. Catal., B*, 2009, **89**, 448.
7 R. Asahi, T. Morikawa, T. Ohwaki, K. Aoki and Y. Taga, *Science*, 2001, **293**, 269.
8 O. Lorret, D. Francová, G. Waldner and N. Stelzer, *Appl. Catal., B*, 2009, **91**, 39.
9 A. Zaleska, E. Grabowska, J. W. Sobczak, M. Gazda and J. Hupka, *Appl. Catal., B*, 2009, **89**, 469.
10 C. K. Xu, R. Killmeyer, M. L. Gray and S. U. M. Khan, *Appl. Catal., B*, 2006, **64**, 312.
11 C. Adán, A. Bahamonde, M. F. García and A. M. Arias, *Appl. Catal., B*, 2007, **72**, 11.
12 A. Kubacka, M. F. García and G. Colón, *J. Catal.*, 2008, **254**, 272.
13 Z. F. Bian, J. Zhu, S. Wang, Y. Cao, X. Qian and H. X. Li, *J. Phys. Chem. C*, 2008, **112**, 6258.
14 W. Zhao, W. H. Ma, C. C. Chen, J. C. Zhao and Z. G. Shuai, *J. Am. Chem. Soc.*, 2004, **126**, 4782.
15 B. F. Gao, Y. J. Kim, A. K. Chakraborty and W. I. Lee, *Appl. Catal., B*, 2008, **83**, 202.
16 X. F. Chen, X. C. Wang, Y. D. Hou, J. H. Huang, L. Wu and X. Z. Fu, *J. Catal.*, 2008, **255**, 59.
17 G. S. Shao, F. Y. Wang, T. Z. Ren, Y. P. Liu and Z. Y. Yuan, *Appl. Catal., B*, 2009, **92**, 61.
18 M. Sathish, B. Viswanathan, R. P. Viswanath and C. S. Gopinath, *Chem. Mater.*, 2005, **17**, 6349.
19 M. Y. Xing, J. L. Zhang and F. Chen, *Appl. Catal., B*, 2009, **89**, 563.
20 S. Sakthivel, M. Janczarek and H. Kisch, *J. Phys. Chem. B*, 2004, **108**, 19384.
21 Y. Cong, J. L. Zhang, F. Chen and M. Anpo, *J. Phys. Chem. C*, 2007, **111**, 6976.
22 T. Ihara, M. Miyoshi, Y. Iriyama, O. Matsumoto and S. Sugihara, *Appl. Catal., B*, 2003, **42**, 403.
23 X. B. Chen and C. Burda, *J. Phys. Chem. B*, 2004, **108**, 15446.
24 X. F. Qiu, Y. X. Zhao and C. Burda, *Adv. Mater.*, 2007, **19**, 3995.
25 Y. Cong, J. L. Zhang, F. Chen, M. Anpo and D. N. He, *J. Phys. Chem. C*, 2007, **111**, 10618.
26 T. C. Jagadale, S. P. Takale, R. S. Sonawane, H. M. Joshi, S. I. Patil, B. B. Kale and S. B. Ogale, *J. Phys. Chem. C*, 2008, **112**, 14595.
27 B. F. Gao, Y. Ma, Y. A. Cao, W. S. Yang and J. N. Yao, *J. Phys. Chem. B*, 2006, **110**, 14391.

28 H. B. Yu, S. Chen, X. Quan, H. M. Zhao and Y. B. Zhang, *Environ. Sci. Technol.*, 2008, **42**, 3791.
29 K. Naeem and F. Ouyang, *E-J. Chem.*, 2009, **6**(S1), S422.
30 M. Anpo, K. Chiba, M. Tomonari, S. Coluccia, M. Che and M. A. Fox, *Bull. Chem. Soc. Jpn.*, 1991, **64**, 543.
31 Y. A. Cao, W. S. Yang, W. F. Zhang, G. Z. Liu and P. Yue, *New J. Chem.*, 2004, **28**, 218.
32 Y. Q. Cao, T. He, L. S. Zhao, E. J. Wang, W. S. Yang and Y. A. Cao, *J. Phys. Chem. C*, 2009, **113**, 18121.
33 E. Arpac, F. Sayılkan, M. Asiltürk, P. Tatar, N. Kiraz and H. Sayılkan, *J. Hazard. Mater.*, 2007, **140**, 69.
34 G. Liu, Y. N Zhao, C. H. Sun, F. Li, G. Q. Lu and H. M. Cheng, *Angew. Chem., Int. Ed.*, 2008, **47**, 4516.
35 D. Li, H. Haneda, S. Hishita and N. Ohashi, *Chem. Mater.*, 2005, **17**, 2588.
36 D. Li, H. Haneda, S. Hishita and N. Ohashi, *Chem. Mater.*, 2005, **17**, 2596.
37 Q. C. Xu, D. V. Wellia, M. A. Sk, K. H. Lim, J. S. C. Loo, D. W. Liao, R. Amal and T. T. Y. Tan, *J. Photochem. Photobiol., A*, 2010, **210**, 181.
38 E. J. Wang, W. S. Yang and Y. A. Cao, *J. Phys. Chem. C*, 2009, **113**, 20912.
39 V. Subramanian, W. W. Burke, H. W. Zhu and B. Q. Wei, *J. Phys. Chem. C*, 2008, **112**, 4550.
40 Y. L. Xu, *The Basics of Semiconducting Oxides and Compounds*, Press of Xi'an Electronic Science and Technology University, Xi'an, 1991, p. 48.
41 N. C. Saha and H. C. Tomkins, *J. Appl. Phys.*, 1992, **72**, 3072.
42 C. S. Gopinath, *J. Phys. Chem. B*, 2006, **110**, 7079.
43 S. Sato, R. Nakamura and S. Abe, *Appl. Catal., A*, 2005, **284**, 131.
44 H. Q. Sun, Y. Bai, H. J. Liu, W. Q. Jin, N. P. Xu, G. J. Chen and B. Q. Xu, *J. Phys. Chem. C*, 2008, **112**, 13304.
45 X. B. Chen, Y. B. Lou, A. C. S. Samia, C. Burda and J. L. Gole, *Adv. Funct. Mater.*, 2005, **15**, 41.
46 Q. C. Xu, D. V. Wellia, R. Amal, D. W. Liao, J. S. C. Loo and T. T. Y. Tan, *Nanoscale*, 2010, **2**, 1122.
47 J. A. Taylor, G. M. Lancaster and J. W. Rabalais, *J. Electron Spectrosc. Relat. Phenom.*, 1978, **13**, 435.
48 T. Lindgren, J. M. Mwabora, E. Avendano, J. Jonsson, A. Hoel, C. G. Granqvist and S. E. Lindquist, *J. Phys. Chem. B*, 2003, **107**, 5709.
49 H. Q. Sun, Y. Bai, W. Q. Jin and N. P. Xu, *Sol. Energy Mater. Sol. Cells*, 2008, **92**, 76.
50 N. Serpone, D. Lawless and R. Khairutdinov, *J. Phys. Chem.*, 1995, **99**, 16655.
51 J. C. Yu, W. Ho, J. Yu, S. K. Hark and K. Iu, *Langmuir*, 2003, **19**, 3889.
52 L. V. Saraf, S. I. Patil, S. B. Ogale, S. R. Sainkar and S. T. Kshirsager, *Int. J. Mod. Phys. B*, 1998, **12**, 2635.

